machines

MDPI

Article

Vibration Attenuation in Particle Mixer Using Magnetorheological Damping Technology to Mitigate the Brazil Nut Effect

Kwon Joong Son

Department of Mechanical and Design Engineering, Hongik University, Sejong 30016, Republic of Korea; kjson@hongik.ac.kr

Abstract: In industrial particle mixing processes, vibrations can intensify the Brazil nut effect (BNE), resulting in larger particles ascending, which contributes to vertical segregation based on particle size differences. These vibrations arise due to mass imbalance, motor functioning, and external disturbances, which negatively influence the efficiency of mixing. This research employs magnetorheological (MR) damping technology to reduce vibration-induced particle separation and consequently diminish the BNE. A drum mixer with an integrated MR damper was designed and constructed for experimental purposes, and its effectiveness in reducing vibrations was evaluated. Furthermore, simulations using the discrete element method (DEM) were performed to study the decrease in the BNE in different vibration settings. The results demonstrated that MR damping effectively decreased vibration levels, which significantly diminished the BNE and maintained the consistency of particle mixing. This study demonstrates the potential of MR damping as a practical solution to enhance mixing performance in industrial applications.

Keywords: magnetorheological damper; Brazil nut effect; discrete element method; particle mixing; vibration suppression

check for updates

Academic Editors: Jian Yang, Lei Deng and Wenxing Li

Received: 3 May 2025
Revised: 31 May 2025
Accepted: 3 June 2025
Published: 4 June 2025

Citation: Son, K.J. Vibration Attenuation in Particle Mixer Using Magnetorheological Damping Technology to Mitigatethe Brazil Nut Effect. *Machines* **2025**, *13*, 487. https://doi.org/10.3390/machines13060487

Copyright: © 2025 by the author. Licensee MDPI, Basel, Switzerland. This article is an open access article distributed under the terms and conditions of the Creative Commons Attribution (CC BY) license (https://creativecommons.org/licenses/by/4.0/).

1. Introduction

The homogeneous mixing of organic and inorganic granular materials is a critical process in various manufacturing industries, including semiconductor fabrication, battery production, pharmaceuticals, material processing, construction, and food manufacturing. The fundamental principle of particle mixing involves inducing flow in an initially heterogeneous particle system to enhance entropy and achieve a more uniform distribution. This is typically achieved by imparting motion to the particle container, using blending structures such as rotating blades, or employing a combination of both [1–6]. Although mechanical agitation generally improves the homogeneity of the mixture, unintended particle segregation can occur under certain conditions. For example, in drum mixers, differences in the particle size or specific aspect ratio of the drum container can lead to axial or radial segregation, affecting the overall efficiency and uniformity of the mixing process [7–17].

Extensive research has been devoted to elucidating the mechanisms behind axial and radial segregation during particle mixing. Kuo et al. [18] experimentally demonstrated axial segregation induced by both size and other factors in drum mixers, facilitated by the mixing of glass beads of various sizes and materials with differing elasticity, such as glass and rubber balls. Lin et al. [19] explored binary particle mixing in rotating drums through a combination of DEM simulations and a Gaussian process model, leading to an optimized structural design that enhances mixing efficiency while reducing segregation. Miao et al. [20] investigated how

axial segregation characteristics influence the particle collision energy in rotating drums, with a focus on particle properties and drum geometry. Liao and Zhang [21] examined how the shape of particles affects density-induced segregation and dynamic behavior within rotating drums, underscoring the importance of the morphology of the particles. He et al. [22] examined how increasing the size of rotating drums influences flow behavior and the role of size-induced segregation. Finally, Kumar et al. [23] investigated the integration of machine learning with DEM simulations to predict segregation behavior to optimize mixing performance in rotating drums.

One of the most prominent segregation phenomena, apart from axial and radial segregation, is the BNE. When vibrational loads are applied to granular materials, larger particles tend to migrate upward against gravity. This phenomenon is named after the tendency for the largest Brazil nuts to ascend to the top when a container containing mixed nuts is shaken during transportation and handling [24,25]. In industrial settings, BNE can adversely influence mixing uniformity by inducing unintended particle segregation, which, in turn, diminishes both process efficiency and consistency. Extensive experimental and numerical studies have investigated its underlying mechanisms. Schröter et al. [26] systematically analyzed the BNE and its counterpart, the reverse Brazil nut effect (RBNE), in vertically vibrated binary granular mixtures. By varying parameters such as the vibration frequency, amplitude, and particle size ratio, they provided information on the fundamental mechanisms governing size segregation. Gajjar et al. [27] employed time-resolved three-dimensional (3D) images to observe the upward migration of larger particles in shaken granular materials, demonstrating the critical role of the shape and orientation of particles in segregation. Van der Linden et al. [28] investigated the BNE in colloidal systems without external agitation, showing that Brownian motion and electrostatic interactions alone could drive larger particles to the surface. Maurel et al. [29] examined the relevance of the BNE in regolith grains on asteroid surfaces, revealing that repeated shaking events cause larger particles to migrate upward, which has implications for planetary surface evolution. Furthermore, Kruppa et al. [30] explored the BNE in mixtures with long-range repulsive interactions using both computational simulations and theoretical analysis. Their findings suggest that interparticle interactions, alongside gravitational effects, influence segregation dynamics in various physical systems, including colloidal suspensions and plasmas.

Despite these advancements, previous research has focused predominantly on idealized experimental conditions or simplified models. The primary motivation for this study is the insufficient investigation into the BNE induced by base excitation. The impact of base vibrations on industrial-scale granular mixing systems remains insufficiently explored. In practical industrial environments, mixing systems are subject to various external vibrations induced by surrounding machinery, leading to fluctuating excitation frequencies and amplitudes. These vibrations can intensify particle segregation, decreasing mixing efficiency and product uniformity [31,32]. However, effective mitigation strategies specifically designed for the base-excited BNE remain underdeveloped. Addressing this gap, the present study explores the application of MR damping technology as a means of vibration suppression to mitigate the BNE in industrial particle mixers. By integrating MR dampers into the system, this research aims to improve mixing performance and minimize segregation effects, offering a novel vibration control solution tailored for industrial applications [33–36]. Alternative semi-active damping technologies such as electrorheological (ER) dampers and pneumatic dampers have been employed in vibration control systems, as documented by [37]. ER dampers adjust their rheological properties when subjected to electric fields, while pneumatic dampers control damping by adjusting air pressure. Although these technologies offer certain advantages, MR dampers possess notably faster response times

and deliver higher damping forces, making them especially beneficial for dynamic and high-performance vibration mitigation in systems with high particle density.

This study aimed to enhance particle mixing performance by mitigating vibration-induced segregation through the application of an MR damper, a representative semi-active damping technology. To achieve this, both experimental and numerical approaches were employed to evaluate the vibration attenuation capacity of the MR damper and to analyze changes in particle behavior under different vibration conditions. The scope of this research includes experimental validation using a drum mixer, a widely used industrial particle mixing system. Artificial base excitation was applied to investigate its impact on particle mixing and to assess the effectiveness of the MR damper in suppressing vibrations. Furthermore, DEM simulations were conducted to quantitatively analyze the BNE and other particle-scale behaviors induced by base excitation. These simulations provide valuable mechanical insights that are difficult to obtain solely through experiments. The findings of this study contribute to the development of practical vibration control strategies for industrial particle mixers, ensuring improved mixing uniformity and reduced particle segregation. The integration of MR damping technology offers a promising approach for optimizing mixing efficiency in various industrial applications.

The principal contributions of this research include the developing an experimental drum mixer platform integrated with an MR damper to minimize vibrations, conducting a hybrid analysis that combines experimental approaches with DEM to study the BNE in varying excitation and damping contexts, and identifying essential vibration parameters and damping conditions critical for controlling segregation in industrial particle mixing systems.

The remainder of this paper is organized as follows. Section 2 outlines the materials and methodology, including the characteristics and control of the MR damper, the experimental setup of a drum mixer with base excitation, and the DEM modeling and simulation configurations. Section 3 presents the experimental and simulation results, analyzing the effects of the base excitation and magnetization of the MR damper on the particle mixing performance. The discussion highlights the role of the damper in mitigating vibration-induced segregation. Section 4 concludes the study by summarizing its contributions, assessing industrial applicability, and suggesting future research directions.

2. Materials and Methods

2.1. MR Damper and Control System

In this study, an MR damper, a type of smart damper, was used to mitigate the base vibrations applied to the particle mixer. Unlike passive dampers, an MR damper allows for real-time control of the damping coefficient, enabling it to respond effectively to a wider range of vibration frequencies and amplitudes [38]. Due to their adaptability and high level of responsiveness, MR dampers have been widely used in vibration control applications for automotive suspension [39], aircraft components [40], and structures related to civil engineering and defensive protection [41–45]. These applications take advantage of the damper's ability to dynamically adjust to changing vibration conditions while maintaining stability and improving performance.

An MR damper operates using a suspension fluid composed of an oil-based medium dispersed with micro-scale magnetically responsive particles [46,47], as illustrated in Figure 1a. When no external magnetic field is applied, the MR fluid behaves as a Newtonian fluid, exhibiting constant viscosity, irrespective of the applied shear rate. However, upon application of an external magnetic field, the particles align along the magnetic flux lines and form columnar structures [48], as illustrated in Figure 1b. This alignment results in an increase in resistance to shear deformation, effectively introducing yield stress into the system. The

fluid then exhibits characteristics similar to those of a Bingham plastic fluid, where it resists flow until the applied shear stress exceeds a certain threshold [45,49]. As the strength of the magnetic field increases, the yield stress of the MR fluid increases until it reaches saturation. Upon yielding, the fluid enters a shear flow stage, where its apparent viscosity increases with the strength of the applied magnetic field until it approaches a saturation level. This shear behavior under Couette flow conditions is illustrated in Figure 1c [50,51].

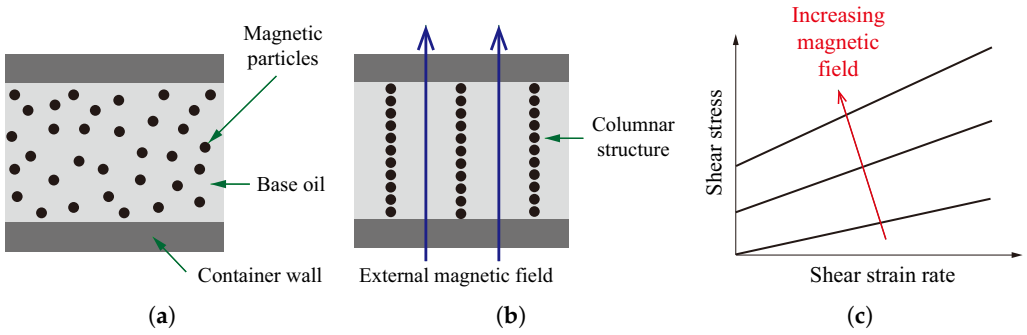


Figure 1. (**a**) MR fluid suspension, (**b**) magnetized MR fluid, and (**c**) Bingham fluid behavior.

A typical MR damper consists of several key components: a cylinder, piston, electromagnetic coil, and the MR fluid itself. The piston is equipped with orifice holes that allow the MR fluid to flow as it moves reciprocally within the cylinder [52]. The electromagnetic coil, wound around the piston, generates a magnetic field in response to an applied current, dynamically adjusting the viscosity of the MR fluid in real time. As the strength of the magnetic field increases, the viscosity of the fluid increases, increasing the damping force [53]. This adaptive behavior allows the damper to efficiently control vibrations and absorb shocks, making it highly suitable for industrial applications where precise and rapid adjustments are required [54].

To attenuate base excitation vibrations in the particle mixer, this study employed Lord Corporation MR Damper Model RD-8041-1, a semi-active MR damper designed for precise vibration control. Manufactured by Lord Corporation in Baltimore, MD, USA, this model features a stroke length of 74 mm and is widely used in vibration isolation and motion control applications. The RD-8041-1 damper operates using MR fluid, a suspension of micrometer-sized magnetically responsive particles dispersed in a carrier oil. When an external magnetic field is applied, the MR fluid undergoes a rapid transition from a Newtonian to a Bingham plastic state, increasing its yield stress and enabling tunable damping force modulation. This real-time adaptability makes the RD-8041-1 particularly effective in controlling vibration-induced segregation in particle mixers. The technical specifications of the damper are summarized in Table 1.

Table 1. Key specifications of the Lord Corporation MR Damper RD-8041-1.

Specification [1]	Unit	Value
Stroke distance	mm	74.0
Max tensile strength	N	8896
Max continuous current (30 s max)	A	1
Max intermittent current (short bursts)	A	2
Magnetized damping force (5 cm/s @ 1 A)	N	2447
Non-magnetized damping force (20 cm/s)	N	667

[1] Specifications are based on the manufacturer's technical data sheet.

The modeling results of the Lord MR RD-8041-1 damper highlight the strong dependence of its viscous damping coefficient and yielding force on the strength of the applied magnetic

field. Numerical and experimental analyses confirm that the damping coefficient increases nonlinearly with the intensity of the magnetic field, as the magnetized MR fluid undergoes a phase transition from a Newtonian to a Bingham plastic state. This transition leads to a rapid increase in the yield stress, which is directly correlated with the yield force of the damper, enabling greater resistance to motion. As the current supplied to the electromagnet increases, the chain-like structures of the magnetic particles within the MR fluid, as illustrated in Figure 1b, become more rigid, enhancing the energy dissipation capacity of the damper. Beyond a certain threshold, however, the damping force reaches a saturation point, where further increases in the strength of the magnetic field result in diminishing returns in yield-stress amplification. These insights demonstrate that precise control of the magnetic field enables tunable damping characteristics, allowing the damper to transition from a low-resistance, underdamped state to a high-resistance, critically overdamped condition, making it highly adaptable for semi-active suspension applications [55,56].

To regulate the intensity of the magnetic field and control the damping characteristics of the RD-8041-1, a Lord Wonder Box is utilized. This proprietary control unit, also developed by Lord Corporation, is specifically designed for MR damper applications. The Wonder Box precisely adjusts the electrical current supplied to the electromagnetic coil of the damper, modifying the rheological properties of the MR fluid in real time. By enabling closed-loop or open-loop control configurations, the Wonder Box enhances vibration suppression efficiency, making it well-suited for applications requiring adaptive damping in dynamic environments.

In addition, a vibration sensing system is integrated into the setup to monitor real-time oscillations within the particle mixer. The SW-420 vibration detection sensor module (manufactured by Seeed Studio located in Senzhen, China) is used for this purpose, detecting external vibrations and providing the corresponding digital signal output. The vibration detection signal acquired from the vibration detection sensor can be applied in the implementation of feedback control, allowing the MR damper to autonomously react to base excitation situations. This combination of an MR damper, intelligent control unit, and vibration sensor ensures effective suppression of vibration-induced disturbances, thereby improving mixing uniformity and minimizing unwanted particle segregation. Figure 2 illustrates the integrated arrangement of the MR damper, the driver that supplies current to the coil of the MR damper to modulate the damping characteristic, the vibration sensor, and the microcontroller (Model Arduino Uno, manufactured by Arduino Srl in Monza, Italy) responsible for the control of the MR damper.

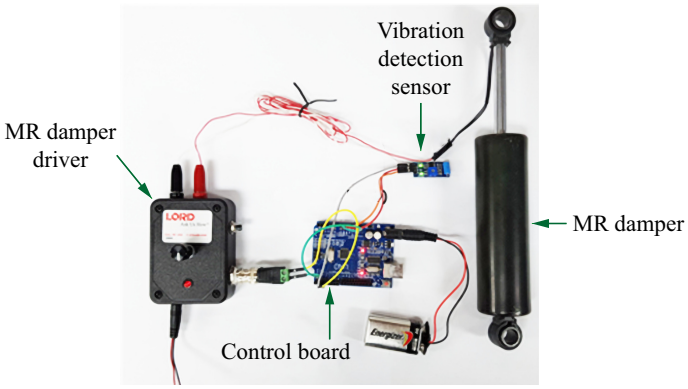


Figure 2. MR damper and control system consisting of control board, MR damper driver, and vibration detection sensor.

2.2. Vibration Experiment of Drum Mixer with MR Damper

An experimental setup was devised to examine how base excitation influences the mixing efficiency of a drum mixer using the BNE and to evaluate the capability of a semi-

active MR damper in reducing particle segregation due to the BNE. This setup includes a drum mixer driven by an electric motor to enable precise base excitation, along with an MR damper designed to modify damping properties. Various mixing experiments were conducted under different vibrational scenarios to evaluate the correlation between vibration control and particle mix uniformity.

The basic structure of the experimental setup consists of a rectangular C-shaped frame made from 6061-T6 aluminum alloy. The drum mixer is located on the top plate, and the base excitation is provided by an electric motor mounted on the bottom plate. One side of both the top and bottom plates is fixed with a vertical plate, while the other side remains open. At this open end, an MR damper is installed between the top and bottom plates using clevis joints. The MR damper controller, the control board, and the motor driver are located on the bottom plate. Figure 3 displays the assembled experimental setup.

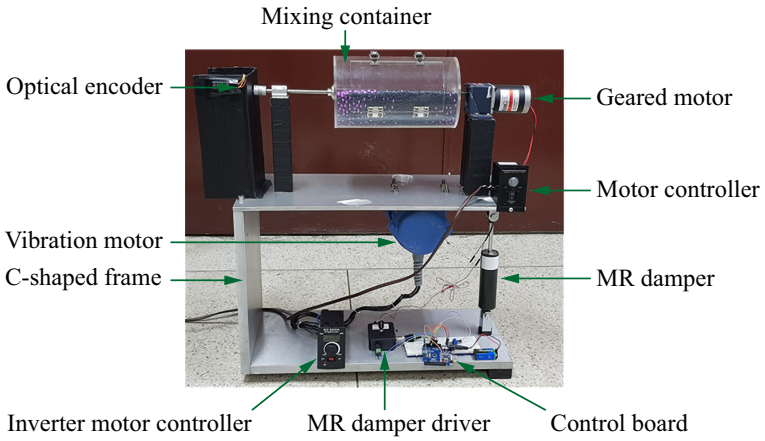


Figure 3. Experimental setup.

The inverter motor (Model HSRV-0152 produced by Sungshin Motor Co., Ltd. in Ansan-si, Republic of Korea) features a rated power of 0.15 kW. It achieves a maximum rotational speed of 3600 rpm and generates an excitation force of 1668 N. This motor is operated by the MX-6000A inverter driver, also manufactured by Sungshin Motor Co. The driver is compatible with a single-phase 220–230 V input at 50/60 Hz and offers an adjustable output voltage between 0 V and 230 V. Its output frequency can vary from 0.5 Hz to 120.0 Hz, with a maximum power output of 400 W.

The drum-mixing container is made of transparent acrylic to allow for visual observation of the particles throughout the mixing procedure. It is cylindrical, with an internal diameter of 14 cm, a length of 26 cm, and a wall thickness of 0.5 cm, as detailed in the work by Alchikh-Sulaiman et al. [57] on experimentation and DEM simulation. The ends of the cylinder are fitted with a geared motor for rotation and an encoder for speed measurement and control. A hinged door on the curved surface of the vessel facilitates the loading of particles. The selected drive motor is a two-pole, 24V, 60-degree geared motor (model D615-30B by DAEHWA E/M Co., Ltd., located in Ansan-si, Republic of Korea). This motor has a gear ratio of 1/50 and delivers a maximum speed of 60 rpm, which accommodates the operational range of 5.5 to 30 rpm used in the study by Alchikh-Sulaiman et al. [57]. An Arduino Uno control board—the same type used for MR damper management—is utilized for the motor's feedback control.

To visually observe the BNE during the mixing process, the experimental particles were selected on the basis of differences in size and color to ensure a clear identification of the segregation behavior. Spherical black beads with a diameter of 3 mm and purple beads with a diameter of 8 mm were chosen for the experiment. A transparent acrylic cylindrical vessel

was loaded with a total of 800 g of particles, comprising 750 g of small particles and 50 g of large particles, which facilitated the clear observation of particle movement and segregation.

The mixing experiments were conducted while rotating the cylindrical vessel at 30 rpm, with variations in base excitation levels and MR damper control settings, as shown in Figure 3. To analyze the effect of vibration on particle segregation, the drum mixer was subjected to three different levels of base excitation, which were controlled by adjusting the rotational speed of the electric motor to 600 rpm, 1200 rpm, and 1800 rpm. By varying the excitation levels, the experiment aimed to assess the influence of vibration intensity on the mixing performance of the drum mixer. The MR damper was controlled using the Wonder Box, which provided six different control voltage levels: 0 V, 1 V, 2 V, 3 V, 4 V, and 5 V. These voltage settings corresponded to damper coil currents of 0 mA, 222 mA, 667 mA, 1111 mA, 1555 mA, and 2000 mA, respectively. By systematically adjusting the voltage input, the experiment examined how different damping forces influenced vibration suppression and particle segregation within the drum mixer. A total of 18 experimental cases were performed, combining the three base excitation levels with the six MR damper settings. The vibration amplitude on the vessel support proximal to the MR damper was quantified for each experimental scenario using a 3-axis piezoelectric vibrometer (model AV-160D, produced by Guangzhou Amittari Instruments Co., Ltd., located in Guangzhou, China). This instrument operates within a frequency range of 10 Hz to 1 kHz and accommodates displacement measurements spanning 0.001 to 4.000 mm. The experiments aimed to evaluate the effectiveness of vibration suppression in reducing BNE-induced particle segregation and to determine the extent to which controlled damping could enhance mixing uniformity. The results were analyzed based on visual observations and quantitative measurements of particle distribution under varying vibration and damping conditions.

2.3. DEM Modeling and Simulation

The discrete element method is a numerical technique used to analyze the flow characteristics of a particle system on the particle scale by calculating the dynamic behavior and contact interactions of individual particles [58–61]. In experimental methods, only the boundary particles on the outer surface of the system can be visually observed, making it extremely difficult to track kinematic variables such as the position and velocity of individual particles in real time. In contrast, DEM simulation provides detailed data on the position, velocity, and contact forces of the particles, enabling a more comprehensive and quantitative evaluation of the mixing behavior and particle interactions. This enhances the understanding of particle processing mechanisms and allows for improved process optimization.

In this study, DEM simulations were conducted under mixing and base excitation conditions similar to the experimental setup described in Section 2.2. The theoretical background and formalization of DEM are not covered in detail in this paper. Instead, the focus is on the simulation procedure, the contact model, and the parameter settings. Readers seeking more detailed information on the theoretical formulation of the DEM are referred to [62,63] for additional reference.

The calculation domain in the DEM model includes both the particles and the cylindrical vessel. The contact forces influencing the motion of individual particles arise from interactions with other particles or contact with the inner wall of the vessel. The cylindrical vessel used in the DEM simulation has the same internal dimensions as the experimental vessel, with an inner diameter of 14 cm and a length of 26 cm. The particles used in the DEM simulation were generated to match the experimental conditions, consisting of black particles with a diameter of 3 mm and purple particles with a diameter of 8 mm. The black and purple particles weighed 750 g and 50 g, respectively, consistent with the experimental setup.

The mixing conditions in the DEM simulation were set to match the experimental conditions, with the cylindrical vessel rotating at a constant speed of 30 rpm on its central axis. Base excitation was implemented by applying a sinusoidal motion in the direction of the gravitational field, simulating the effect of base excitation observed in the experiment. The amplitude of the sinusoidal motion was determined using the measured values obtained from the vibration sensor installed on the experimental setup.

In order to calculate the contact force between cohesionless particles, the widely used Hertz–Mindlin (HM) model was adopted in this study. This specific contact model was selected for its precision in capturing the nonlinear elastic response due to contact overlaps, a critical aspect in realistic particle interaction simulations. Unlike traditional linear spring–dashpot models, this model accurately reflects the increase in contact forces with deformation. In addition, it incorporates material properties such as the elastic modulus, Poisson ratio, friction coefficient, and restitution coefficient, which are available or can be measured experimentally. In this study, where the particle diameters were 3 and 8 mm, the effects of cohesion and adhesion were negligible, making the HM model ideal for modeling the non-cohesive nature of the granular system.

Figure 4 illustrates the contact condition between two spherical particles (i and j) in the DEM, showing a normal overlap (δ_n) on the contact surface with a contact radius of a.

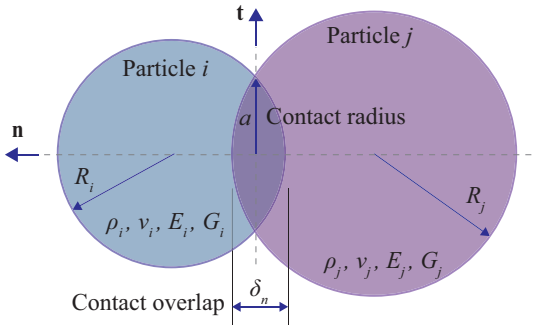


Figure 4. Schematic of two particles in contact and the associated Hertz–Mindlin contact model parameters.

The Hertz–Mindlin model calculates the contact forces between the particles, including the normal elastic force ($\mathbf{F}_n^e$), the normal damping force ($\mathbf{F}_n^v$), and the cohesive force ($\mathbf{F}_n^c$) along the normal direction ($\hat{\mathbf{n}}$). In the tangential direction ($\hat{\mathbf{t}}$), the elastic force ($\mathbf{F}_t^e$) and the viscous damping force ($\mathbf{F}_t^v$) are considered. The boldface symbols represent vector quantities, while italicized characters denote scalars. A haton a vector indicates a unit vector with a magnitude of one. The components of the contact forces are defined as follows:

$$\mathbf{F}_n^e = \frac{4}{3}\sqrt{R_{\text{eq}}E_{\text{eq}}^2}\delta_n^{3/2}\hat{\mathbf{n}}, \tag{1}$$

$$\mathbf{F}_n^v = -\sqrt{\frac{20}{3}}\left(\frac{\ln e}{\ln^2 e + \pi^2}\right)\left(m_{\text{eq}}^2 R_{\text{eq}}E_{\text{eq}}^2\delta_n\right)^{1/4}(\mathbf{v}_{\text{rel}}\cdot\hat{\mathbf{n}})\hat{\mathbf{n}}, \tag{2}$$

$$\mathbf{F}_n^c = -4\sqrt{\pi\gamma E_{\text{eq}}}a^{3/2}\hat{\mathbf{n}}, \tag{3}$$

$$\mathbf{F}_t^e = -8\sqrt{R_{\text{eq}}G_{\text{eq}}^2\delta_n}\delta_t\hat{\mathbf{t}}, \tag{4}$$

$$\mathbf{F}_t^v = -\sqrt{\frac{80}{3}}\left(\frac{\ln e}{\ln^2 e + \pi^2}\right)\left(m_{\text{eq}}^2 R_{\text{eq}}G_{\text{eq}}^2\delta_n\right)^{1/4}(\mathbf{v}_{\text{rel}}\cdot\hat{\mathbf{t}})\hat{\mathbf{t}}, \tag{5}$$

where R_{eq} is the equivalent particle radius, E_{eq} is the equivalent Young's modulus, δ_n is the normal overlap distance, e is the coefficient of restitution, m_{eq} is the equivalent particle mass, $\mathbf{v}_{\text{rel}}$ is the relative velocity between the contacting particles, γ is the cohesive surface energy, a is the contact radius, G_{eq} is the equivalent shear modulus, and δ_t is the

accumulated tangential displacement during contact. The equivalent material properties are determined as follows:

$$R_{\text{eq}} = \left(\frac{1}{R_i} + \frac{1}{R_j} \right)^{-1}, \tag{6}$$

$$m_{\text{eq}} = \left(\frac{1}{m_i} + \frac{1}{m_j} \right)^{-1}, \tag{7}$$

$$E_{\text{eq}} = \left(\frac{1-\nu_i^2}{E_i} + \frac{1-\nu_j^2}{E_j} \right)^{-1}, \tag{8}$$

$$G_{\text{eq}} = \left(\frac{2-\nu_i}{G_i} + \frac{2-\nu_j}{G_j} \right)^{-1}, \tag{9}$$

where R_i and R_j are the radii of the particles i and j, m_i and m_j are the particle masses, E_i and E_j are the elastic moduli, G_i and G_j are the shear moduli, and ν_i and ν_j are the Poisson ratios of the contact particles.

In addition to translational forces, the rolling friction ($\mathbf{M}_r$) associated with the rotational motion of the particles is defined as follows:

$$\mathbf{M}_r = -\mu_r |\mathbf{F}_n| R\boldsymbol{\omega}, \tag{10}$$

where μ_r is the coefficient of rolling friction, $|\mathbf{F}_n|$ is the magnitude of the normal contact force, and $\boldsymbol{\omega}$ is the relative angular velocity vector.

The Hertz–Mindlin contact model effectively captures the dynamic behavior of granular systems by considering both normal and tangential forces, as well as viscoelastic interactions and rolling resistance. This model provides a robust framework for simulating complex particle dynamics in DEM-based studies.

The material constants [64] and contact model parameters [65] required for the contact model are summarized in Table 2. The particle and vessel materials were both set as acrylic, consistent with the experimental setup.

Table 2. Material properties and contact parameters of acrylic for DEM simulation.

Property	Unit	Value
Density	kg/m^3	1250
Modulus of elasticity	MPa	300
Poisson's ratio	-	0.4
Coefficient of lateral friction	-	0.39
Coefficient of rolling friction	-	0.000271
Coefficient of restitution	-	0.55

By combining experimental data with DEM simulations, this study aims to provide deeper insight into the relationship between base excitation and mixing efficiency, as well as to evaluate the potential of using MR dampers to mitigate vibration-induced particle segregation.

3. Results and Discussion

3.1. Experimental Results and Discussion

The mixing experiments used 50 g of 8 mm purple particles and 750 g of 3 mm black particles, which were sequentially introduced into the mixing drum. The drum was rotated at a speed of 30 rpm while base excitation was applied. Figure 5 illustrates the vibration amplitudes measured by the three-axis vibrometer throughout the base excitation tests.

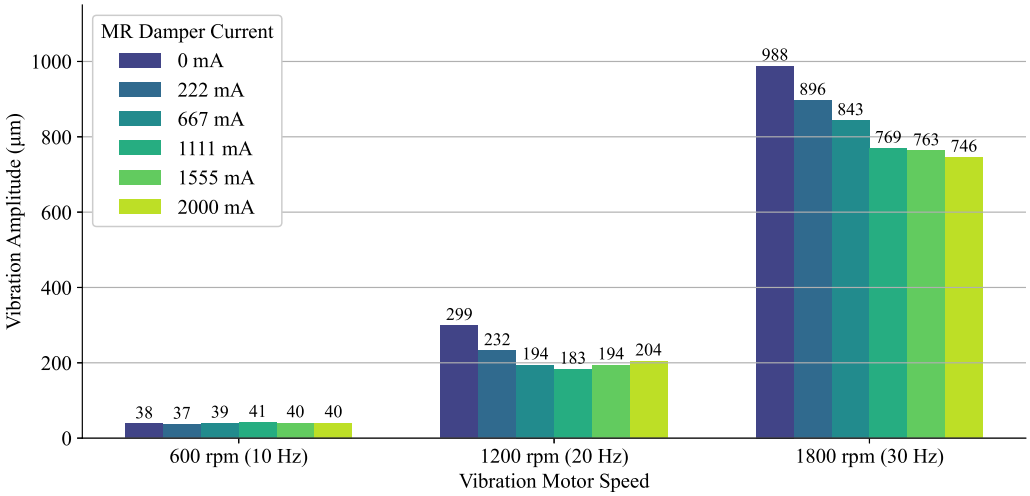


Figure 5. Measured vibration amplitudes at different motor speeds and MR damper driving voltages.

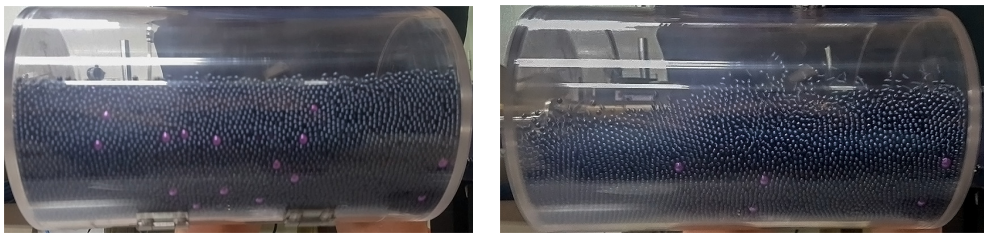
At a motor speed of 600 rpm, the vibration amplitude measured within the C frame was approximately 39 µm. The standard deviation of the vibration amplitude, in varying MR damper currents, was 1.47 µm, indicating a minor variation in amplitude as the damper current changed. This suggests that the influence of the MR damper on vibration mitigation is minimal at lower excitation levels.

At a rotor speed of 1200 rpm, the maximum vibration amplitude increased significantly to 300 µm, which is nearly 7.7 times higher than the amplitude measured at 600 rpm. The amplitude response induced by the modulating currents of the MR damper exhibited a concave downward trend, with the minimum vibration amplitude of 183 µm observed at a 3 V input to the Wonder Box. This represents a 39% decrease compared to the maximum vibration amplitude, demonstrating the potential of the MR damper for efficient vibration reduction at moderate excitation levels.

When the motor accelerated to 1800 rpm, the maximum vibration amplitude increased to 988 µm, with an average amplitude of 834 µm. Increasing the MR damper current resulted in a reduction in the vibration amplitude. The minimum observed vibration amplitude was 746 µm with a 5 V input signal to the Wonder Box, representing a reduction of 10.6% from the maximum vibration amplitude.

In the absence of any vibration, a typical pattern of particle movement was observed during the mixing process in a drum. The interaction between the particles and the internal surface of the drum led to an upward movement of the particles in the direction of drum rotation. Upon reaching the free surface, the particles moved down the slope, promoting the mixing action. When larger particles were included among smaller ones, radial segregation occurred, wherein the larger particles were pushed towards the outer wall, preventing them from moving into the central region of the particle bed.

At speeds around 1800 rpm, significant vibrations resulted in noticeable changes in behavior. These vibrations led to the particles repeatedly detaching from the vessel wall, reducing the effectiveness of friction force transmission over time. This phenomenon significantly decreased particle movement along the central axis of the drum's rotation. While smaller particles displayed minor swirling near the wall of the vessel, larger particles did not emulate this motion. Instead, because of the BNE, they tended to ascend vertically. Therefore, when observed along the horizontal plane of the cylindrical surface of the drum, larger particles appeared less frequently than in the condition without vibration, as illustrated in Figure 6. This suggests that the larger particles were elevated toward the free surface rather than adhering to the drum wall.



(**a**) (**b**)

Figure 6. Particles viewed horizontally from the front (**a**) without vibration and (**b**) with vibration.

Increasing the strength of the magnetic field of the MR damper's internal coil resulted in an elevated damping coefficient, which effectively diminished the vibration amplitude and mitigated the BNE. The correlation between reduced vibration and improved mixing performance due to the suppression of the BNE was further assessed using DEM simulation, as discussed in Section 3.2.

3.2. Simulation Results and Discussion

To investigate the influence of base excitation and MR damping on the dynamics of particle mixing and segregation, DEM simulations were performed under five different scenarios. EDEM commercial software (version 2022.2, Altair Engineering Inc., Troy, MI, USA) was used to execute all simulations, and data analysis was carried out using its Python-based post-processing library, EDEMpy. Furthermore, generative artificial intelligence tool ChatGPT (Version GPT-4o, OpenAI, San Francisco, CA, USA) served as a supplementary coding assistant to support the development of Python scripts for data analysis and visualization.

In addition to the baseline simulation without vibration, four additional cases involving base excitation were simulated. Based on the experimental results, which showed significant changes in particle behavior at motor speeds of 1200 rpm and 1800 rpm, two simulations were performed for each condition: one without activation of the MR damper and another under the minimum vibration amplitude achieved by applying the optimal damper current. The particle system comprised 750 g of 3 mm black particles and 50 g of 8 mm purple particles, consistent with the experimental conditions.

In all scenarios, the cylindrical vessel rotated steadily at 30 rpm. The simulations considered conditions with and without base excitation and evaluated the effects of applying current to the MR damper during vibrations. To isolate the influence of vibration alone and eliminate the effects of drum-induced particle flow, the cylindrical vessel was rotated, together with base excitation, for up to 10 s, after which the rotation was stopped while vibration was applied continuously for the remainder of the simulation. Base excitation was implemented by applying sinusoidal movement in the vertical plane. The parameters of this excitation—specifically, frequency and amplitude—were derived from the experimental data shown in Figure 3, which is associated with electric motor speeds of 1200 rpm and 1800 rpm. These speeds correspond to radial frequencies of approximately 20 Hz and 30 Hz, respectively.

Figure 7 illustrates simulation snapshots from both front and top views, captured at 5 s intervals over a 20 s period without any vibration. In this control scenario, typical drum-mixing particle flow dynamics were observable, including particle cascading and radial segregation, where larger particles tended to remain closer to the outer boundary. To investigate surface geometry in this scenario, protractor overlays were applied to front-view images taken at 5 s and 15 s to approximate the angle of repose. Under active rotation at 30 rpm, the free surface formed a stable inclined layer with an approximate angle of

25°, resulting from the combined frictional interactions among the particles and between the particles and the wall of the container. Once the drum stopped rotating, the free surface gradually adjusted to a less steep profile, reducing the angle of repose to about 18°. This slope development represents the dynamic equilibrium achieved by shear-induced particle rearrangement and the resistance from interfacial friction within the rotating vessel. Upon stopping the drum rotation at 10 s, the base excitation also stopped, which did not cause further alterations in the particle mixing state. This indicates the absence of vibration-related processes such as the BNE.

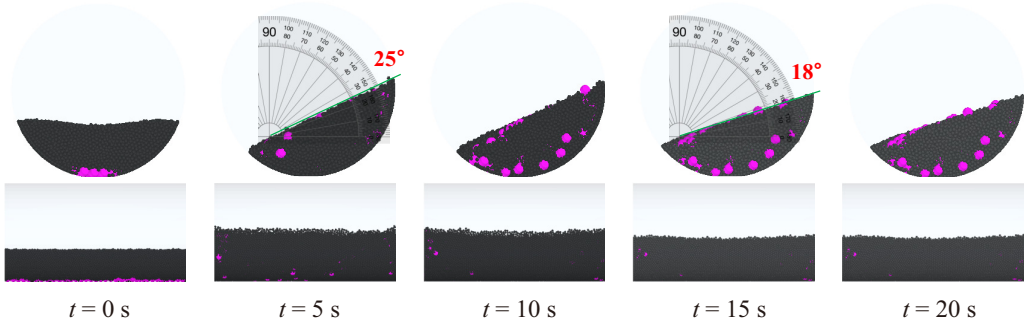


Figure 7. Results of DEM simulations for drum mixing without base excitation over a duration of 20 s, captured at 5 s intervals from both front and top perspectives.

Figure 8 presents the results of the simulation operating under a 20 Hz base excitation with an amplitude of 299 µm, corresponding to a motor speed of 1200 rpm, without activating the MR damper at a driving current of 0 mA. The angle of repose, derived from front-view images captured at 5 and 15 s, indicated that during drum rotation, the dynamic angle remained around 25°, while it decreased to approximately 17° once the rotation ceased. In the baseline scenario without vibration, the static repose angle was 18°. The slight decrease in slope indicates that the periodic detachment of particles from the drum wall, induced by vibrations, temporarily reduces the contact forces between the wall and particles. Consequently, there is a minor decrease in the average friction resistance, which contributes to a lower effective angle of repose when vibrations are present. Nonetheless, it appears that the BNE was not detected during the observation.

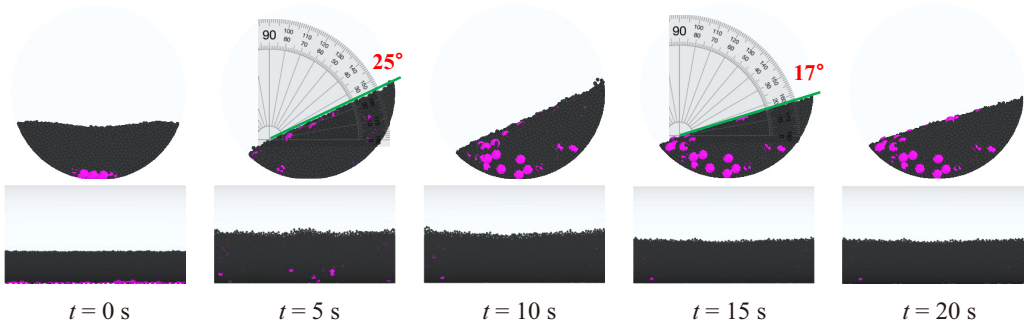


Figure 8. DEM simulation results for drum mixing with a 20 Hz base excitation frequency and a 299 µm amplitude over 20 s, recorded every 5 s from front and top views.

Figure 9 presents the simulation executed at a consistent base excitation frequency of 20 Hz, with the MR damper activated by a current of 1111 mA, achieving a reduced vibration amplitude of 183 µm. Activation of the MR damper led to a decrease in vibration amplitude, but the particle behavior closely resembled the undamped scenario depicted in Figure 8, with BNE notably absent. In addition, the angle-of-repose values were consistent, suggesting that the damping effect had a negligible influence on particle segregation under this level of moderate excitation.

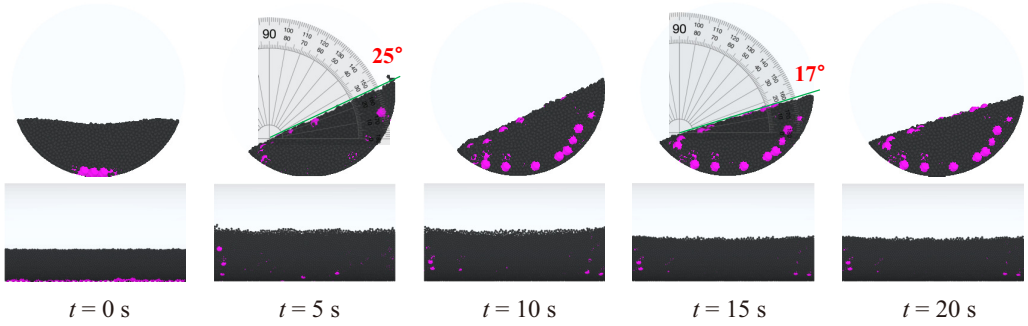


Figure 9. DEM simulation data of drum mixing featuring a 20 Hz base excitation with an amplitude of 183 µm for 20 s, using an MR damper at 1111 mA to decrease the amplitude, with recordings captured every 5 s from the front and top perspectives.

Figure 10 displays the simulation results for higher intensity excitation operating at a frequency of 30 Hz with an amplitude of 988 µm, which corresponds to a motor speed of 1800 rpm without MR damping. Throughout the drum-spinning phase, the dynamic angle of repose was observed to be approximately 17°, representing a 32% decrease from the 25° observed in the previous three trials. Upon stopping of the drum rotation, the free surface became perfectly horizontal, resulting in a static repose angle of 0°. This significant decrease in surface inclination is attributed to the high frequency and amplitude of the vibrations, which substantially lowered the effective friction between the particle bed and the drum wall. As a result, reduced wall–particle friction significantly impeded the swirling motion that usually facilitates particle mixing during drum rotation, while BNE became more pronounced due to increased particle detachment and upward movement.

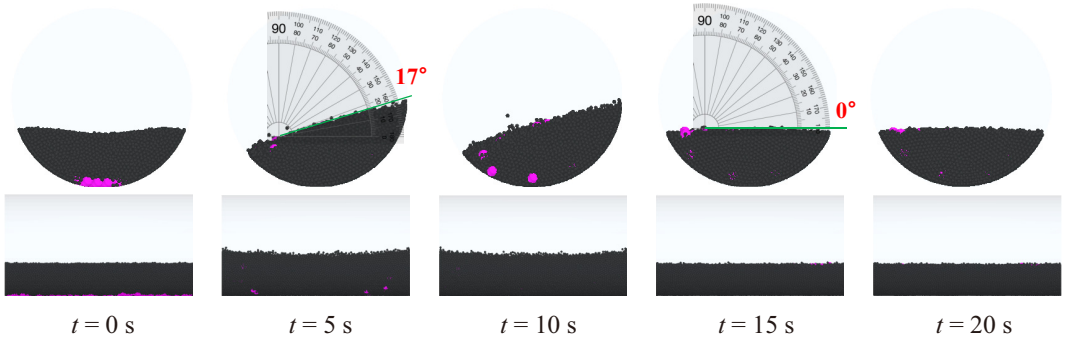


Figure 10. DEM simulation results of drum mixing at a 30 Hz frequency and 988 µm amplitude observed from front and top views every 5 s over 20 s.

Figure 11 demonstrates the scenario in which the MR damper current was adjusted to 2000 mA, achieving a decreased vibration amplitude of 746 µm at 30 Hz. In the presence of MR damping, the dynamic angle of repose observed during drum rotation was 18°, indicating a minor increase of 1° compared to the undamped condition. This suggests a moderate enhancement in the effective friction between the particle bed and the drum surface. Once rotation ceased, the free surface flattened completely, resulting in a static repose angle of 0°. While simulation animations revealed a minor qualitative decline in the BNE, visual inspection is insufficient for definitive evaluation, which requires further comprehensive quantitative analysis.

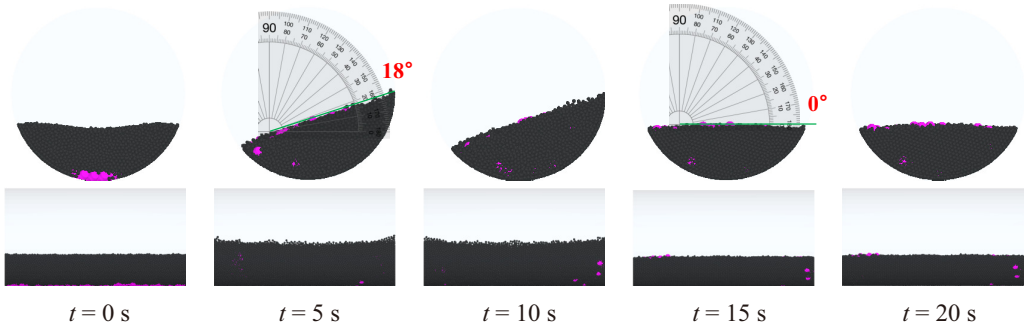


Figure 11. Drum-mixing DEM simulation with 30 Hz base excitation and 746 µm peak amplitude for 20 s, reduced by an MR damper at 2000 mA; recordings taken every 5 s from front and top views.

In DEM-based simulations for mixing processes, the Lacey index is frequently used as a statistical metric to assess variations in particle concentration, serving as an indicator of mixing uniformity [60,66]. However, in this study, the Lacey index was inadequate in accounting for the upward migration of several large particles, which initially settled near the free surface as a result of radial segregation, mainly due to the significant disparity in the number of large particles (150) compared to small particles (42,442). Therefore, as an alternative, the vertical displacement of a probe particle was used as a more direct metric. Specifically, to quantitatively assess the degree of the BNE under different conditions of motor excitation and MR damper functionality, the vertical displacement of a specified probe particle within the larger ensemble was monitored after stopping drum rotation. In particle mixtures, those near the free surface initially exhibited constrained upward motion due to the BNE. The study concentrated on behavior resulting from vibration by designating the probe particle as the sizable particle situated at the lowest vertical position at the start of the phase where only vibration was applied. This selection was made at 11 s, after sufficient realignment and settling of particles following the cessation of drum rotation, rather than precisely at 10 s when the rotation initially stopped. The vertical displacement trajectory of the probe particle in each vibrating simulation is presented in Figure 12.

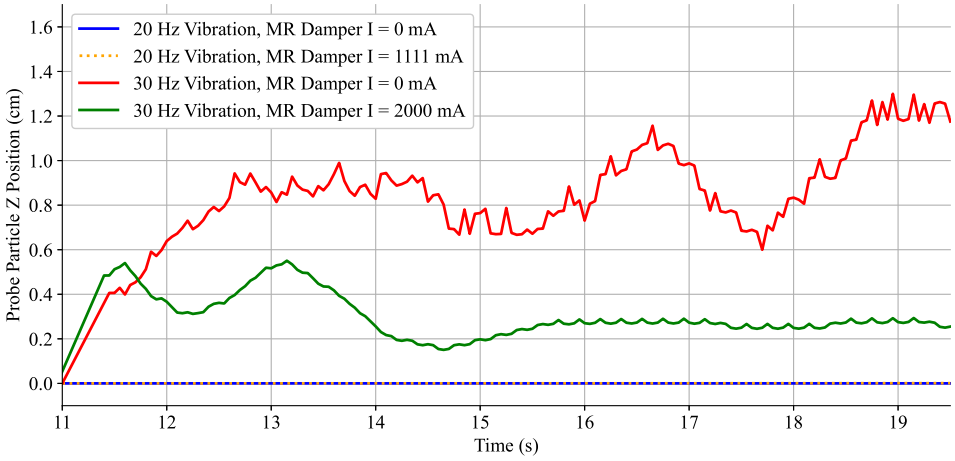


Figure 12. Time evolution of vertical displacement of a probe particle defined as the lowest 8 mm particle at 11 s after flow flattening following the stopping of the drum at 10 s for four vibrating DEM cases.

Since the motion of the probe particle under vibration inherently exhibits significant fluctuations due to transient contacts and collisions, a smoothed rendition of the raw simulation data is shown in Figure 12. To obtain a comprehensible signal while preserving the integrity of the initial conditions, a hybrid smoothing approach was employed. This

method combines a conventional moving average filter, which is effective in reducing high-frequency noise, with an initial localized linear correction. The correction ensures that the smoothed curve matches the initial value precisely by interpolating the first few data points between the original data and the filtered trend. Through this approach, the physical accuracy at the onset of the vibration-only phase is maintained, while a stable depiction of long-term displacement behavior is achieved without the boundary artifacts typically introduced by conventional filtering techniques.

The vertical position of the probe particle over time is depicted in Figure 12. This particle becomes the lowest large particle at 11 s, post settlement of all particles due to the drum's slowing down. The graph presents outcomes for four different vibration conditions, with probe paths refined via the previously discussed hybrid smoothing method. Under a 20 Hz base excitation, equivalent to a motor speed of 1200 rpm, with a vibration amplitude below 300 µm, the probe particle does not show an observable rise, regardless of the MR damper being powered. This indicates that with relatively low excitation conditions, the BNE is negligible, and damping control has a minimal effect.

At a frequency of 30 Hz base excitation, which corresponds to a motor operating at 1800 rpm, the vibration amplitude is approximately 1 mm. This level of vibration causes the probe particle to display a significant and gradual upward movement, demonstrating a pronounced BNE. However, with the MR damper activated at its highest current of 2000 mA, the vibration amplitude is reduced to 746 µm, which significantly reduces the BNE. The probe particle still moves upward, but its displacement is markedly reduced compared to the case without damping. This result shows that diminishing the vibration amplitude effectively mitigates particle segregation due to the BNE.

The findings illustrate a distinct association between the level of base excitation, the role of MR dampers, and the segregation dynamics. The results reveal that the semi-active MR damper plays a pivotal role in controlling the BNE by modulating the vibration amplitude reaching the particle bed. By decreasing dynamic agitation, the damper limits the relative movement among the particles, thereby restricting the convective and percolation processes that lead to the rise of larger particles. Hence, employing MR damping offers an efficient strategy to improve mixing uniformity in vibrated granular systems, particularly in situations where reducing segregation is critical due to external or transport-induced vibration.

Although there have been significant advancements, practical challenges still hinder the deployment of this technology in real-world scenarios. For it to be integrated into industrial environments, the technology needs driver systems that are compact, robust, and easy to integrate with existing mechanical systems. In addition, reliable feedback control algorithms capable of adapting to dynamically changing operating conditions are required. It is also vital to assess the maintenance requirements and cost effectiveness of MR fluid systems, especially for long-term or large-scale use. Advances in intelligent sensing technologies and adaptive closed-loop control systems will be crucial to establishing this vibration suppression method as a viable industrial solution. In particular, an adaptive closed-loop damping system can monitor vibrations in real time and dynamically adjust the input current to the MR damper, thereby maintaining optimal damping performance despite fluctuating external forces.

4. Conclusions

This research investigated how to minimize vibration-induced segregation in a rotating drum mixer by employing a semi-active MR damper, with a focus on the BNE. The study combined physical experiments and DEM simulations to examine how changes in base excitation frequency and amplitude influenced particle segregation and to evaluate the effectiveness of MR damping. At high excitation levels—namely, base vibrations of 30 Hz with nearly

1 mm amplitudes—larger particles exhibited the upward movement characteristic of the BNE, resulting in less uniform mixing. However, by maximizing the input current to the MR damper, the vibration amplitude was significantly reduced, effectively curtailing segregation. DEM simulations corroborated these findings by showing that the vertical movement of large probe particles decreased under damped conditions, highlighting a definitive relationship between decreased vibration and improved mixing performance. These findings indicate that MR dampers can actively manage vibrational energy within the particle bed, thereby limiting size-based segregation driven by convective and percolative processes.

Integrating MR damping technology into vibratory mixing systems offers an efficient strategy to maintain uniformity in the processing of granular materials, specifically in environments where vibrations from external or operational sources are unavoidable. This research illustrates the practical effectiveness of MR dampers in reducing the BNE and emphasizes their adaptability to various excitation scenarios. Future investigations should aim to extend these findings by examining a broader spectrum of particle sizes, shapes, and densities, as well as evaluating different mixing-vessel designs and vibration directions. Furthermore, expanding this study to incorporate advanced control strategies, such as feedback-based real-time current modulation and machine learning-driven vibration state predictions, could enhance the practical use of MR damping systems in industrial mixing operations that demand consistent quality under dynamic operating conditions.

Funding: This research was supported by the Basic Science Research Program through the National Research Foundation of Korea (NRF), funded by the Ministry of Education (No. RS-2022-NR075787). This work was also supported by the 2025 Hongik University Research Fund.

Institutional Review Board Statement: Not applicable.

Informed Consent Statement: Not applicable.

Data Availability Statement: The original contributions presented in this study are included in the article. Further inquiries can be directed to the corresponding author.

Acknowledgments: During the preparation of this manuscript, the author used ChatGPT (OpenAI, GPT-4o, version as of May 2025) for the purpose of assisting in the generation of Python scripts used to analyze DEM simulation data and produce graphical results. The author has reviewed and edited the output and takes full responsibility for the content of this publication.

Conflicts of Interest: The author declares no conflicts of interest.

References

1. Harnby, N. An Engineering View of Pharmaceutical Powder Mixing. *Pharm. Sci. Technol. Today* **2000**, *3*, 303–309. [CrossRef]
2. Pernenkil, L.; Cooney, C.L. A Review on the Continuous Blending of Powders. *Chem. Eng. Sci.* **2006**, *61*, 720–742. [CrossRef]
3. Bauman, I.; Ćurić, D.; Boban, M. Mixing of Solids in Different Mixing Devices. *Sadhana* **2008**, *33*, 721–731. [CrossRef]
4. Bridgwater, J. Mixing of Powders and Granular Materials by Mechanical Means—A Perspective. *Particuology* **2012**, *10*, 397–427. [CrossRef]
5. Huang, A.N.; Kuo, H.P. Developments in the Tools for the Investigation of Mixing in Particulate Systems—A Review. *Adv. Powder Technol.* **2014**, *25*, 163–173. [CrossRef]
6. Asachi, M.; Nourafkan, E.; Hassanpour, A. A Review of Current Techniques for the Evaluation of Powder Mixing. *Adv. Powder Technol.* **2018**, *29*, 1525–1549. [CrossRef]
7. Kuo, H.; Hsu, R.; Hsiao, Y. Investigation of Axial Segregation in a Rotating Drum. *Powder Technol.* **2005**, *153*, 196–203. [CrossRef]
8. He, Y.; Chen, H.; Ding, Y.; Lickiss, B. Solids Motion and Segregation of Binary Mixtures in a Rotating Drum Mixer. *Chem. Eng. Res. Des.* **2007**, *85*, 963–973. [CrossRef]
9. Jiang, M.; Zhao, Y.; Liu, G.; Zheng, J. Enhancing Mixing of Particles by Baffles in a Rotating Drum Mixer. *Particuology* **2011**, *9*, 270–278. [CrossRef]
10. Alizadeh, E.; Dubé, O.; Bertrand, F.; Chaouki, J. Characterization of Mixing and Size Segregation in a Rotating Drum by a Particle Tracking Method. *AIChE J.* **2013**, *59*, 1894–1905. [CrossRef]

11. Yamamoto, M.; Ishihara, S.; Kano, J. Evaluation of Particle Density Effect for Mixing Behavior in a Rotating Drum Mixer by DEM Simulation. *Adv. Powder Technol.* **2016**, *27*, 864–870. [CrossRef]
12. Deng, R.; Tan, Y.; Zhang, H.; Xiao, X.; Jiang, S. Experimental and DEM Studies on the Transition of Axial Segregation in a Truck Mixer. *Powder Technol.* **2017**, *314*, 148–163. [CrossRef]
13. Yang, S.; Sun, Y.; Zhang, L.; Chew, J.W. Segregation Dynamics of a Binary-Size Mixture in a Three-Dimensional Rotating Drum. *Chem. Eng. Sci.* **2017**, *172*, 652–666. [CrossRef]
14. He, S.; Gan, J.; Pinson, D.; Zhou, Z. Particle Shape-Induced Radial Segregation of Binary Mixtures in a Rotating Drum. *Powder Technol.* **2019**, *341*, 157–166. [CrossRef]
15. Huang, P.; Miao, Q.; Ding, Y.; Sang, G.; Jia, M. Research on Surface Segregation and Overall Segregation of Particles in a Rotating Drum Based on Stacked Image. *Powder Technol.* **2021**, *382*, 162–172. [CrossRef]
16. Huang, A.; Cheng, T.; Hsu, W.; Huang, C.; Kuo, H. DEM Study of Particle Segregation in a Rotating Drum with Internal Diameter Variations. *Powder Technol.* **2021**, *378*, 430–440. [CrossRef]
17. Miao, Q.; Huang, P.; Ding, Y.; Guo, J.; Jia, M. Particle Mixing and Segregation Behaviors in the Rotating Drums with Adjacent Axial Segmentations in Different Speed Directions. *Powder Technol.* **2022**, *405*, 117534. [CrossRef]
18. Kuo, H.; Hsiao, Y.; Shih, P. A Study of the Axial Segregation in a Rotating Drum Using Deformable Particles. *Powder Technol.* **2006**, *166*, 161–166. [CrossRef]
19. Lin, L.; Zhang, X.; Yu, M.; Mujtaba, I.M.; Chen, X. Optimized Structure Design for Binary Particle Mixing in Rotating Drums Using a Combined DEM and Gaussian Process-Based Model. *Digit. Chem. Eng.* **2024**, *12*, 100175. [CrossRef]
20. Miao, Q.; Zhu, W.; Ding, Y.; Huang, P.; Hu, C.; Ge, Y. Impact of Axial Segregation Characteristics on the Particle Collision Energy in Rotating Drums. *Miner. Eng.* **2024**, *218*, 109015. [CrossRef]
21. Liao, C.C.; Zhang, Z.H. Experimental Investigate the Influences of Particle Shape on Density-Induced Segregation and Dynamic Properties in Binary Granular Mixture in a Rotating Drum. *Powder Technol.* **2025**, *454*, 120696. [CrossRef]
22. He, J.; Wang, Y.; Yang, L.; Zheng, Q.; Xu, J.; Liu, S.; Zhou, Z. Similarity Analysis of Size-Induced Segregation and Flow Behavior during the Scaling up Process of Rotating Drums. *Powder Technol.* **2024**, *448*, 120252. [CrossRef]
23. Kumar, S.; Garg, Y.; Khatoon, S.; Dubey, P.; Kumari, K.; Anand, A. Predicting Mixing: A Strategy for Integrating Machine Learning and Discrete Element Method. *Ind. Eng. Chem. Res.* **2024**, *63*, 19640–19661. [CrossRef]
24. Dai, S.; Zhang, S.; Gao, F.; He, X.; Sheng, D. Investigation of Particle Segregation in a Vertically Vibrated Binary Mixture: Segregation Process and Mechanism. *Comput. Geotech.* **2024**, *169*, 106236. [CrossRef]
25. Dai, S.; Shan, F.; Xiong, H.; Zhang, S.; He, X.; Sheng, D. Evolution of Pore Structure and Flow Properties in Particle Segregation. *J. Hydrol.* **2025**, *652*, 132651. [CrossRef]
26. Schröter, M.; Ulrich, S.; Kreft, J.; Swift, J.B.; Swinney, H.L. Mechanisms in the Size Segregation of a Binary Granular Mixture. *Phys. Rev. E* **2006**, *74*, 011307. [CrossRef]
27. Gajjar, P.; Johnson, C.G.; Carr, J.; Chrispeels, K.; Gray, J.M.N.T.; Withers, P.J. Size Segregation of Irregular Granular Materials Captured by Time-Resolved 3D Imaging. *Sci. Rep.* **2021**, *11*, 8352. [CrossRef]
28. van der Linden, M.N.; Everts, J.C.; van Roij, R.; van Blaaderen, A. Realization of the Brazil-nut Effect in Charged Colloids without External Driving. *Proc. Natl. Acad. Sci. USA* **2023**, *120*, e2213044120. [CrossRef] [PubMed]
29. Maurel, C.; Ballouz, R.L.; Richardson, D.C.; Michel, P.; Schwartz, S.R. Numerical Simulations of Oscillation-Driven Regolith Motion: Brazil-nut Effect. *Mon. Not. R. Astron. Soc.* **2017**, *464*, 2866–2881. [CrossRef]
30. Kruppa, T.; Neuhaus, T.; Messina, R.; Löwen, H. Soft Repulsive Mixtures under Gravity: Brazil-nut Effect, Depletion Bubbles, Boundary Layering, Nonequilibrium Shaking. *J. Chem. Phys.* **2012**, *136*, 134106. [CrossRef]
31. Liao, C.C.; Hsiau, S.S. Transport Properties and Segregation Phenomena in Vibrating Granular Beds. *KONA Powder Part. J.* **2016**, *33*, 109–126. [CrossRef]
32. Qiao, J.; Duan, C.; Dong, K.; Wang, W.; Jiang, H.; Zhu, H.; Zhao, Y. DEM Study of Segregation Degree and Velocity of Binary Granular Mixtures Subject to Vibration. *Powder Technol.* **2021**, *382*, 107–117. [CrossRef]
33. Choi, S.B.; Li, W.; Yu, M.; Du, H.; Fu, J.; Do, P.X. State of the Art of Control Schemes for Smart Systems Featuring Magneto-Rheological Materials. *Smart Mater. Struct.* **2016**, *25*, 043001. [CrossRef]
34. Gopinath, B.; Sathishkumar, G.; Karthik, P.; Martin Charles, M.; Ashok, K.; Ibrahim, M.; Mohamed Akheel, M. A Systematic Study of the Impact of Additives on Structural and Mechanical Properties of Magnetorheological Fluids. *Mater. Today Proc.* **2021**, *37*, 1721–1728. [CrossRef]
35. Huang, X.; Yang, B. Towards Novel Energy Shunt Inspired Vibration Suppression Techniques: Principles, Designs and Applications. *Mech. Syst. Signal Process.* **2023**, *182*, 109496. [CrossRef]
36. Sharma, S.K.; Sharma, R.C.; Upadhyay, R.K.; Lee, J. Enhanced Ship Engine Vibration Reduction Using Magnetorheological Dampers and Adaptive Neuro-Fuzzy Control System. *Ships Offshore Struct.* **2025**, *20*, 143–159. [CrossRef]
37. Wang, Z.; Liu, C.; Zheng, X.; Zhao, L.; Qiu, Y. Advancements in Semi-Active Automotive Suspension Systems with Magnetorheological Dampers: A Review. *Appl. Sci.* **2024**, *14*, 7866. [CrossRef]

38. Kumbhar, M.B.; Desavale, R.G.; Jagadeesha, T. Experimentation and Damping Performance Analysis of a MR Damper for Resonance Control in a Quarter Car Suspension System. *J. Vib. Eng. Technol.* **2024**, *12*, 5973–5983. [CrossRef]
39. Zhang, Y.; Guo, J.; Yang, J.; Li, X. Recent Structural Developments and Applications of Magnetorheological Dampers (MRD): A Review. *Magnetochemistry* **2023**, *9*, 90. [CrossRef]
40. Xu, Z.D.; Chen, Z.H.; Huang, X.H.; Zhou, C.Y.; Hu, Z.W.; Yang, Q.H.; Gai, P.P. Recent Advances in Multi-Dimensional Vibration Mitigation Materials and Devices. *Front. Mater.* **2019**, *6*, 143. [CrossRef]
41. Garg, D.P.; Anderson, G.L. Structural Damping and Vibration Control via Smart Sensors and Actuators. *J. Vib. Control.* **2003**, *9*, 1421–1452. [CrossRef]
42. Yu, Y.; Royel, S.; Li, Y.; Li, J.; Yousefi, A.M.; Gu, X.; Li, S.; Li, H. Dynamic Modelling and Control of Shear-Mode Rotational MR Damper for Mitigating Hazard Vibration of Building Structures. *Smart Mater. Struct.* **2020**, *29*, 114006. [CrossRef]
43. Son, K.J.; Fahrenthold, E.P. Evaluation of Magnetorheological Fluid Augmented Fabric as a Fragment Barrier Material. *Smart Mater. Struct.* **2012**, *21*, 075012. [CrossRef]
44. Son, K.J.; Fahrenthold, E.P. Magnetorheological Damping of Fragment Barrier Suspension Systems. *J. Dyn. Syst. Meas. Control.* **2018**, *140*, 091002. [CrossRef]
45. Son, K.J.; Fahrenthold, E.P. Impact Dynamics Simulation for Magnetorheological Fluid Saturated Fabric Barriers. *J. Comput. Nonlinear Dyn.* **2024**, *19*, 061002. [CrossRef]
46. Son, K.J. A Discrete Element Model for the Influence of Surfactants on Sedimentation Characteristics of Magnetorheological Fluids. *Korea-Aust. Rheol. J.* **2018**, *30*, 29–39. [CrossRef]
47. Kumar, V.; Kumar, R.; Kumar, H. Rheological Characterization and Performance Evaluation of Magnetorheological Finishing Fluid. *J. Appl. Fluid Mech.* **2020**, *13*, 185–197. [CrossRef]
48. Saha, P.; Mukherjee, S.; Mandal, K. Rheological Response of Magnetic Fluid Containing Fe3O4 Nano Structures. *J. Magn. Magn. Mater.* **2019**, *484*, 324–328. [CrossRef]
49. Pei, P.; Peng, Y. Constitutive Modeling of Magnetorheological Fluids: A Review. *J. Magn. Magn. Mater.* **2022**, *550*, 169076. [CrossRef]
50. Genç, S.; Phulé, P.P. Rheological Properties of Magnetorheological Fluids. *Smart Mater. Struct.* **2002**, *11*, 140. [CrossRef]
51. Upadhyay, R.V.; Choi, S.B. Modeling, Measurements and Validation of Magnetic Field Dependent Flow Behavior of Magnetorheological Fluids; Static and Dynamic Yield Stress. *Smart Mater. Struct.* **2021**, *30*, 117002. [CrossRef]
52. Zhu, X.; Jing, X.; Cheng, L. Magnetorheological Fluid Dampers: A Review on Structure Design and Analysis. *J. Intell. Mater. Syst. Struct.* **2012**, *23*, 839–873. [CrossRef]
53. Cruze, D.; Hemalatha, G.; Jebadurai, S.V.S.; Sarala, L.; Tensing, D.; Christy, S.S.J.E. A Review on the Magnetorheological Fluid, Damper and Its Applications for Seismic Mitigation. *Civ. Eng. J.* **2018**, *4*, 3058–3074. [CrossRef]
54. Masa'id, A.; Lenggana, B.W.; Ubaidillah, U.; Susilo, D.D.; Choi, S.B. A Review on Vibration Control Strategies Using Magnetorheological Materials Actuators: Application Perspective. *Actuators* **2023**, *12*, 113. [CrossRef]
55. Desai, R.M.; Jamadar, M.E.H.; Kumar, H.; Joladarashi, S.; Rajasekaran, S.C.; Amarnath, G. Evaluation of a Commercial MR Damper for Application in Semi-Active Suspension. *SN Appl. Sci.* **2019**, *1*, 993. [CrossRef]
56. Jamadar, M.e.H.; Desai, R.M.; Saini, R.S.T.; Kumar, H.; Joladarashi, S. Dynamic Analysis of a Quarter Car Model with Semi-Active Seat Suspension Using a Novel Model for Magneto-Rheological (MR) Damper. *J. Vib. Eng. Technol.* **2021**, *9*, 161–176. [CrossRef]
57. Alchikh-Sulaiman, B.; Alian, M.; Ein-Mozaffari, F.; Lohi, A.; Upreti, S.R. Using the Discrete Element Method to Assess the Mixing of Polydisperse Solid Particles in a Rotary Drum. *Particuology* **2016**, *25*, 133–142. [CrossRef]
58. Son, K.J. A Numerical Study of the Influence of Rheology of Cohesive Particles on Blade Free Planetary Mixing. *Korea-Aust. Rheol. J.* **2018**, *30*, 199–209. [CrossRef]
59. Son, K.J. A Numerical Study of the Influence of Operating Conditions of a Blade Free Planetary Mixer on Blending of Cohesive Powders. *Korea-Aust. Rheol. J.* **2019**, *31*, 15–23. [CrossRef]
60. Byun, J.; Son, K.J. Experimental and Numerical Study of Computer Vision-Based Real-Time Monitoring of Polymeric Particle Mixing Process in Rotary Drum. *Polymers* **2024**, *16*, 1524. [CrossRef]
61. Son, K.J. Discrete Element Method Analysis of Soil Penetration Depth Affected by Spreading Speed in Drone-Seeded Rice. *Agriculture* **2025**, *15*, 422. [CrossRef]
62. Fleissner, F.; Gaugele, T.; Eberhard, P. Applications of the Discrete Element Method in Mechanical Engineering. *Multibody Syst. Dyn.* **2007**, *18*, 81–94. [CrossRef]
63. Tavarez, F.A.; Plesha, M.E. Discrete element method for modelling solid and particulate materials. *Int. J. Numer. Methods Eng.* **2007**, *70*, 379–404. [CrossRef]
64. Hlosta, J.; Jezerská, L.; Rozbroj, J.; Žurovec, D.; Nečas, J.; Zegzulka, J. DEM Investigation of the Influence of Particulate Properties and Operating Conditions on the Mixing Process in Rotary Drums: Part 1—Determination of the DEM Parameters and Calibration Process. *Processes* **2020**, *8*, 222. [CrossRef]

65. Höhner, D.; Wirtz, S.; Scherer, V. Experimental and Numerical Investigation on the Influence of Particle Shape and Shape Approximation on Hopper Discharge Using the Discrete Element Method. *Powder Technol.* **2013**, *235*, 614–627. [CrossRef]
66. Wen, Y.; Liu, M.; Liu, B.; Shao, Y. Comparative Study on the Characterization Method of Particle Mixing Index Using DEM Method. *Procedia Eng.* **2015**, *102*, 1630–1642. [CrossRef]

Disclaimer/Publisher's Note: The statements, opinions and data contained in all publications are solely those of the individual author(s) and contributor(s) and not of MDPI and/or the editor(s). MDPI and/or the editor(s) disclaim responsibility for any injury to people or property resulting from any ideas, methods, instructions or products referred to in the content.